

Cathodic Protection of X100 Pipeline Steel in Simulated Soil Solution

Yingchun Chen, Zuquan Wang, Xinhua Wang*, Xuting Song, Cheng Xu

College of Mechanical Engineering and Applied Electronics Technology, Beijing University of Technology, Beijing, China

*E-mail: paper_bgdjd103@163.com

Received: 8 June 2018 / Accepted: 20 July 2018 / Published: 1 September 2018

Generally, the basic parameters of conventional cathodic protection design mostly rely on theoretical or empirical approximate formulas. An over protection phenomenon has emerged for pipeline systems with large scale differences in soil environment. This paper investigated the basic parameters of the electric cathodic protection under three types of simulated soil solution environments (Korla station, Lhasa station and Yingtan station) for X100 high strength pipeline steel by using the technology of electrochemical impedance spectroscopy (EIS) combined with polarization curves. The results showed that the EIS and polarization curves can help determine the basic parameters for X100 high strength pipeline steel cathodic protection under the above three simulated soil solution environments. Also, the changing characteristics of charge transfer resistance (R_t) and cathode potential change (E) changes, can be achieved by fitting EIS results: with negative potential shifting, R_t appeared a maxima value; Hydrogen evolution reaction started at the stage when $R_t < 1000 \Omega \cdot \text{cm}^2$; For X100 high strength pipeline steel under different simulated soil solution environments at Korla station, Lhasa station and Yingtan station, the size of hydrogen evolution potential was successively reduced.

Keywords: X100 pipeline steel; cathodic protection; polarization curves; EIS

1. INTRODUCTION

Recently, the oil & gas pipelines have expanded rapidly in china. These new pipelines are of long transportation distance and go through north, south, east and west of china. As china consists of complex terrain, the external environment of pipeline has a prolonged contact with a variety of soil types. Soil erosion is one of the important underlying factors threatening the safe operation of the pipelines [1]. If a flaw occurs in an in-service pipeline it is likely to cause a huge loss of natural

resources and a lot of environmental pollution. Therefore, underground engineering applications are urgently needed to solve such practical problems [2]. With the growing demand of energy, long distance oil and gas production and transmission has become a necessity. In order to reduce the pipeline construction cost and improve efficiency of transportation, the use of large-diameter high-grade pipeline steel with the ability of handling high-pressures, is an inevitable trend in the development of oil and gas pipelines. Thus study on the X100/X120 high strength steel has obtained high attention among worldwide pipeline research and manufacturing facilities [3-5]. Also, in order to prevent pipeline corrosion and to prolong the service life of the pipeline, cathodic protection is usually adopted in the pipeline service [6,7]. However, the design of basic parameters of conventional cathodic protection mostly relies on the theoretical or empirical approximate formulas which makes the steel very susceptible to the phenomenon of “over protection” or “less protection”. “Over protection” leads to excessive hydrogen evolution at cathode which significantly increases the steel hydrogen embrittlement [8,9]. At the same time, the cathode hydrogen evolution/oxygen reaction occurs on the surface of the metal pipeline, which results in cathodic disbandment of the coating [10-12]. Kamimura [13] pointed out that the cathodic disbanding of the coating was caused by the current flowing through the cathodes leading to the production of a large amount of alkaline substances and H₂. Nielsen [14] found in accordance with field investigations and tests, that the surface of the buried steel pipeline under cathodic protection (CP) generates a large amount of OH⁻ which increases the pH of the environment where the coating defect occurs due to the alkaline environment of buried pipe. Li [15] studied the corrosion of the crevice under cathodic potential. A set of experimental equipment was designed and developed. The influence of CP on the crevice area under the desquamating coating of X70 pipeline steel was studied.

At this stage, proceeding research on the characteristics of how high-strength steel hydrogen evolution occurs under different cathodic protection potential (CPP) and the relationship between pipeline CPP and pipeline hydrogen evolution conditions is necessary. Many experimental works referring to some lower strength levels of pipeline steel report empirical values about the cathodic protection potential and the optimum cathodic protection potential is often defined as 200 mV electronegative than the self-corrosion potential [16]. Zhang [17] used electrochemical methods to study the cathodic polarization behavior of X80 steel in 3% NaCl, and proposed a method for determining cathodic protection parameters through laboratory tests.

However, the prevalent studies on the actual soil environment are not enough, and no simulation of the actual system has been established. Given the complexity of soil conditions, taking X100 high strength steel as study object, three representative simulated soil solution environments Korla station, Lhasa station and Yingtan station were chosen. The effect of three typical simulated soils solution and their cathodic polarization behavior is investigated by using the technology of electrochemical impedance spectroscopy (EIS) combined with polarization curves. The theoretical and experimental results on high-strength steel cathodic protection can fund the fundamental parameters under three typical simulated soil solution environments and provide a reliable theoretical and technical support for the cathodic protection systems engineering.

2. EXPERIMENTAL

2.1 Experimental materials

In this work, X100 pipeline steel was used. The chemical composition of X100 steel is (wt.%): C 0.06, Si 0.26, Mn 1.90, P 0.008, S 0.001, Nb 0.07, Ti 0.01 and Fe balance. X100 pipeline steel with sample size of 10 mm×10 mm×2 mm was used as experimental sample. The copper wire is soldered on one side of the sample, and then the sample is sealed with epoxy resin leaving only the working surface of the sample as shown in Figure 1. Face of the sample sequentially progressive metallographic sandpaper polished like a mirror. After being cleaned by deionized water and acetone, the sample was cold dried and set aside into the dryer.

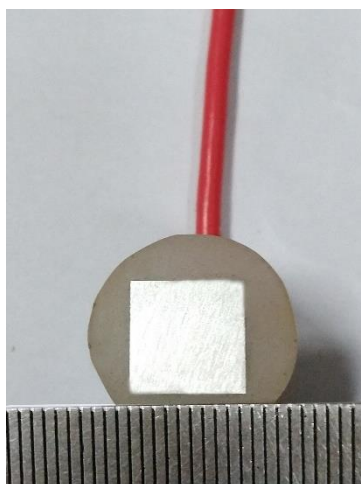


Figure 1. Experimental sample (scale 1mm)

Table 1. Chemical compositions of three kinds of simulated soil solutions (g/L)

Content	pH	CaCl ₂	NaCl	Na ₂ SO ₄	MgSO ₄ ·7H ₂ O	MgCl ₂ ·6H ₂ O	KNO ₃	NaHCO ₃
Korla	9.1	0.2442	3.1707	2.5276	0	0.6699	0.2156	0.1462
Lhasa	6.8	0.081	0	0.012	0.071	0	0.050	0.055
Yingtang	4	0.222	0.936	0.284	0.394	0	0.596	0.302

In order to determine the CPP of X100 steel in different types of soil environment, we selected three typical soil environments in China (data from the National Natural Corrosion Environment Experiment of Beijing University of Science and Technology <http://isisn.nsf.gov.cn/egrantweb/>). These typical soils include Korla station soil, Lhasa station soil and Yingtang station soil. Among them the Korla station soil is alkaline and the salt content is high, which is typical of the desert saline soil in western China; Lhasa station soil is a typical near-neutral soil in southwest China; Yingtang station has a high content of humus acid and CO₂ in the soil and is highly corrosive, which is typical of the acidic

soil in southeast China. The chemical composition required to formulate the three simulated soil solutions is shown in Table 1.

2.2 Electrochemical test

Diagram of the experimental system is as shown in Figure 2. Solatran's Parstat 2273 electrochemical workstation was used for electrochemical test, three electrodes were used during the electrochemical test: X100 high-strength pipeline steel sample as the working electrode (WE); platinum plate as the counter electrode (CE); saturated calomel electrode (SCE) as the reference electrode (RE). Test environments were Korla station simulated soil solution environment, Lhasa station simulated soil solution environment and Yingtian station simulated soil solution environment.

The sample was placed in the electrolysis cell and on waiting for 30 minutes the double electric layer on each electrode surface reaches a stable state for conducting the polarization curve test. In the polarization curve test, kinetic potential scan rate of 0.5 mV/s was used. In the electrochemical impedance spectroscopy (EIS) test, the cathodic polarization potential was applied to the X100 steel sample using the potentiostat module in the electrochemical workstation and then the EIS at different polarization potentials was measured. The scanning frequency range of 10^5 - 10^{-1} Hz was applied while AC sine wave signal amplitude was 10 mV. The EIS data obtained from the experiment was processed and analyzed by Zsimpwin software.

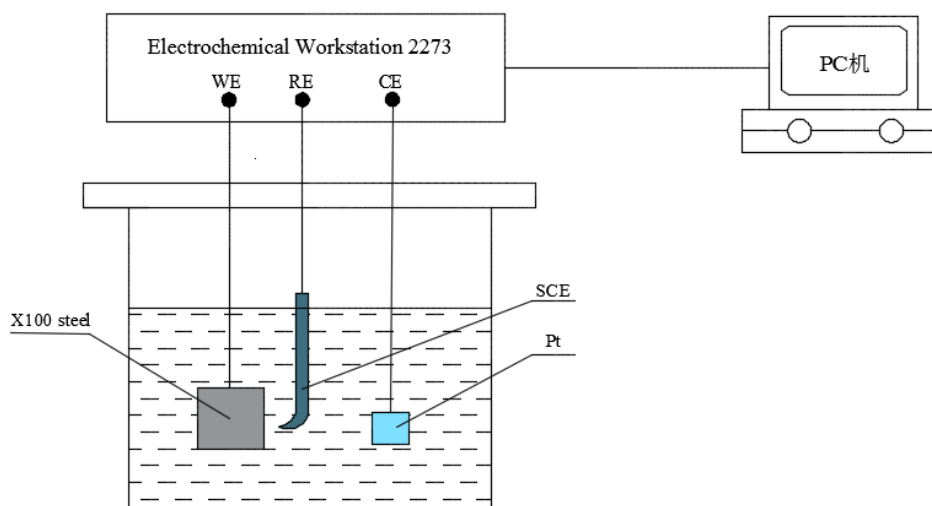


Figure 2. Electrochemical testing device

3. RESULTS AND DISCUSSION

Based on the theoretical analysis of these three types of soil, the cathodic polarization character of the steel under these simulated soil solution environments was studied. The effect of soil types on the pipeline cathodic polarization behavior was discussed so that basic parameters of cathodic

protection under different simulated soil solution environments were theoretically and experimentally obtained.

3.1 Results of the polarization test

Figure 3 shows the polarization curves of X100 pipeline steels under three different simulated soil solution environments. It is obvious that the polarization curves have similar shapes and two inflection points *a* and *b* are present. The portion of the polarization curve above the point *a* is characterized as the anodic polarization, and the portion below the point *a* belongs to the cathodic polarization. In the *a-b* section, the cathodic potential shifts negatively and the cathode current density is quite stable. At this time a large amount of electrons are accumulated on the cathode which strengthens its polarization and protects the metal. When the potential is negative to point *b*, the cathodic current density increases sharply and the magnitude of negative shift of the cathode potential is not large. Hydrogen bubbles appear on the surface of the pipeline steel which is not conducive to metal protection.

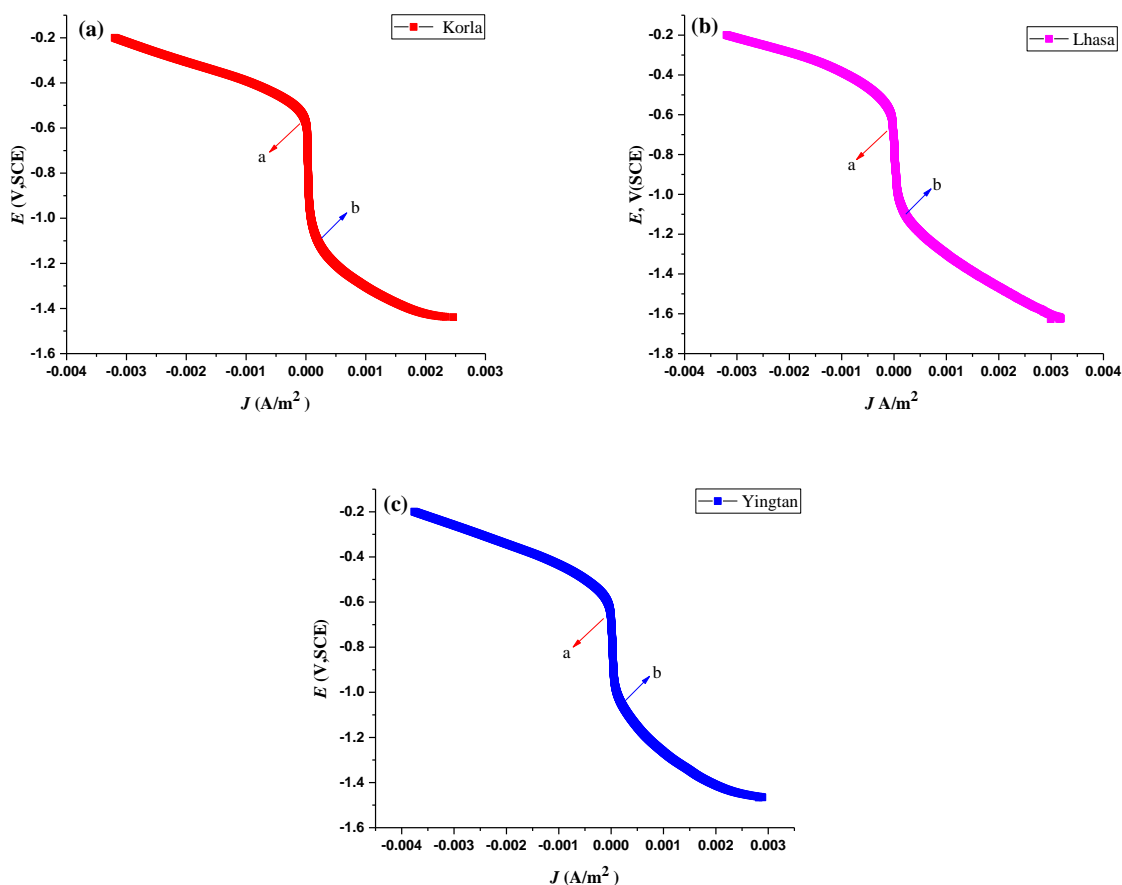
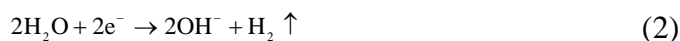


Figure 3. Polarization curves of X100 samples in (a) Korla simulated soil solution, (b) Lhasa simulated soil solution, (c) Yingtan simulated soil solution.

Therefore, the inflection point *a* is a turning point in the transition from oxygen activation control to oxygen diffusion control and this result can be explained by equation (1). The second

inflection point *b* is the turning point of the control of the diffusion of oxygen into the depolarization control of hydrogen. After the second point *b* the hydrogen depolarization can be expressed by equation (2) [18,19].



From the curves above, it is obvious that the cathodic protection potential range of X100 steel under three different environments range from -600 mV~-1150 mV, -650 mV~-1100 mV and -650 mV~-1100 mV respectively. Because the protection potential range is extensive, it is necessary to combine the impedance spectra to obtain the accurate cathodic protection parameters.

3.2 The EIS analysis

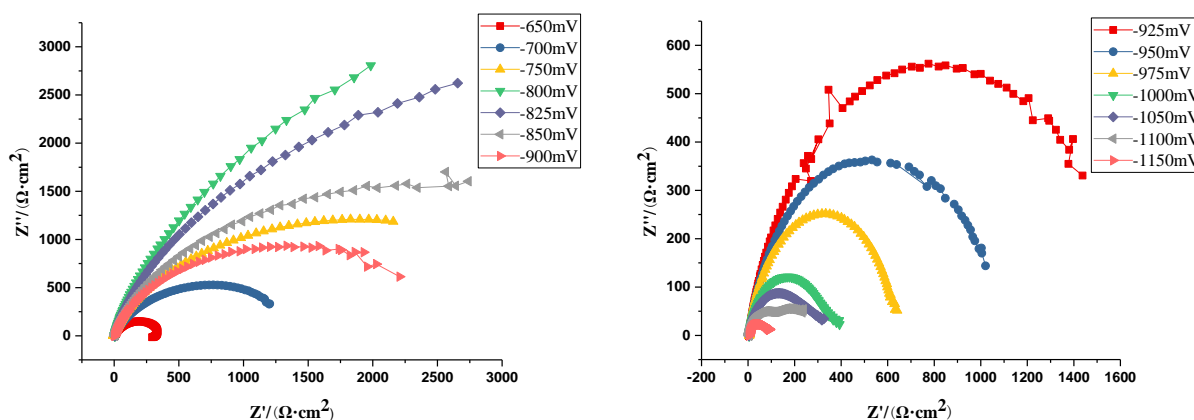


Figure 4. Nyquist diagram of X100 steel at different cathodic polarization potentials in Korla simulated soil solution

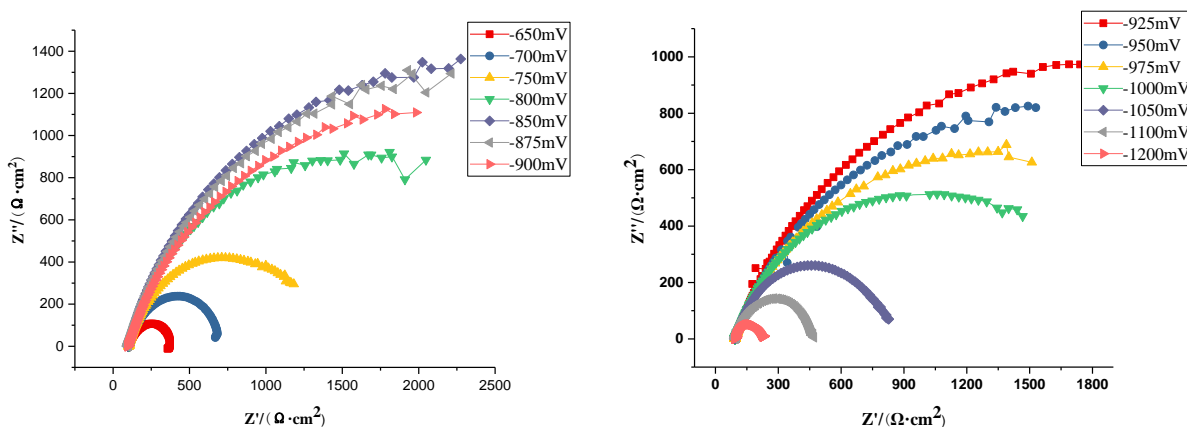


Figure 5. Nyquist diagram of X100 steel at different cathodic polarization potentials in Lhasa simulated soil solution

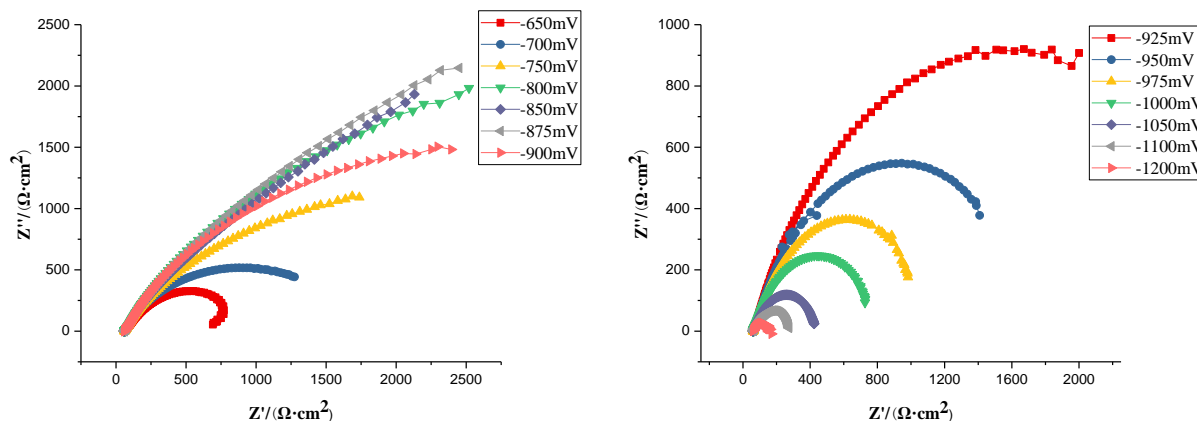


Figure 6. Nyquist diagram of X100 steel at different cathodic polarization potentials in Yingtan simulated soil solution

The pH of the solution has a large effect on the cathodic protection potential of the pipeline steel. Zhang [17] studied the effect of pH on the cathodic protection potential of X80 steel by electrochemical method. He found that the higher the pH value of the same solution, the more negative the optimal cathodic protection potential of X80 steel. China has a vast territory and more complex soil environment. In this paper, the EIS tests were performed under different cathodic polarization potentials (CPP) to further study the X100 steel's cathodic polarization characters under Korla, Lhasa and Yingtan simulated soil solution environments.

The results are shown in Figure 4. According to the results the Nyquist diagram consists of two parts: the first one has high frequency parts which have changed slightly; the other one has low frequency parts which have changed noticeably. The phenomena shows that the combination layer of corrosion products and soil changes slightly and the charge transfer resistance (R_t) changes regularly with the change in CP. R_t can reflect the corrosion rate of the sample where the low-frequency impedance spectra showed that the resistance appears into a maxima value with the decreasing of CPP. Thus the optimal protection potential can be obtained by the regulation of polarization between R_t and CP.

The EIS corresponding equivalent circuit is showed in Figure 7 based on the theoretical analysis [20-22]. In the circuit L represents inductive reactance, R_s represents solution medium resistance, Q_1 and R_1 represent capacitance and resistance of the corrosion product bonding layer. Q_2 and R_t are the electric double layer capacitance and the charge transfer resistance of the metal/solution interface. Due to the EIS "dispersion effect" [23] the capacitance is not ideal in the actual situation where the constant phase angle Q is used instead of the capacitance C to reflect the electrochemical information more accurately. Cao [20] pointed out that the charge transfer resistor R_t responds to the difficulty of the charge transfer process through the interface between the metal/solution interface when the potential is E. Smaller the value of R_t easier is the charge transfer process. Zsimpwin software was used to fit and analyse the EIS results of X100 steel according to the equivalent circuit model, and then the law for variation of R_t versus E (cathode polarization potential) in three soil simulation solutions was obtained, as are shown in Figure 8.

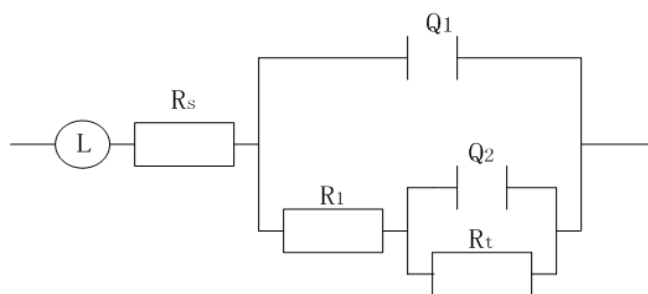


Figure 7. EIS equivalent circuit model

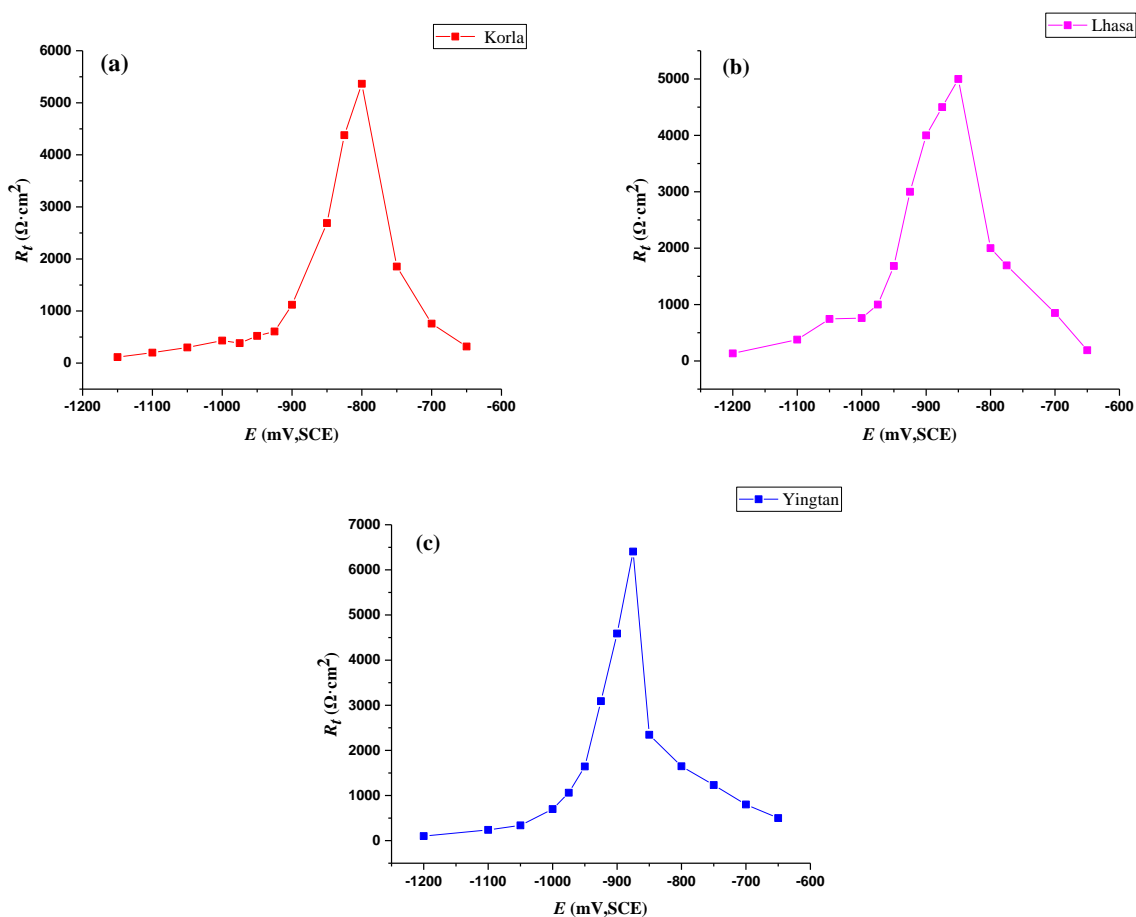


Figure 8. R_t - E curves of X100 samples: (a) Korla simulated soil solution, (b) Lhasa simulated soil solution, (c) Yingtan simulated soil solution.

At the self-corrosion potential, two electrode reactions performed at the same time were the anode reaction and cathode reaction. The impedance information measured at the self-corrosion potential was the result of the mixed of cathode and anode reactions. According to electrochemical theory the cathode and anode reactions proceed simultaneously under mixed potential. The analytical formula of the impedance spectrum under mixed potential is as follows [20]:

$$1/R_t = 1/R_{t,a} + 1/R_{t,c} \tag{3}$$

Where, R_t represents the charge transfer resistance of the metal/solution interface; $R_{t,a}$ represents the anodic reaction's charge transfer resistance; $R_{t,c}$ represents the cathodic reaction's charge transfer resistance

$R_{t,a}$ rises with the negative shift of electrode potential when cathodic polarization is added to the electrodes. However, due to the activation of oxygen in the electrochemical process, the value of $R_{t,c}$ slowly decreases. At this point in time the equivalent circuit of electrode reaction under self-corrosion potential is shown in Figure 9. However, when the cathodic polarization potential is negatively shifted to a certain potential, in addition to the cathodic reduction reaction of oxygen, a cathodic reduction reaction of hydrogen also occurs. In this case the equivalent circuit of electrode reaction under a certain polarization potential is shown in Figure 10. The impedance spectroscopy equation is expressed as following [24-26]:

$$1/R_{t,c} = 1/R_{t,o} + 1/R_{t,H} \tag{4}$$

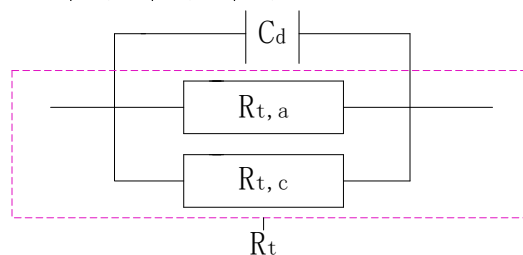


Figure 9. Equivalent circuit diagram of electrode reaction under self-corrosion potential

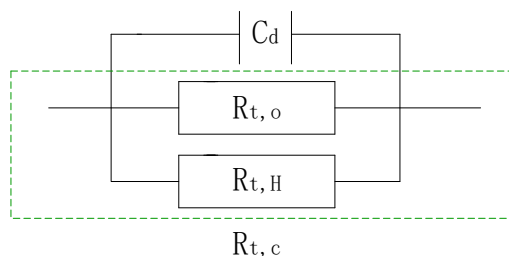


Figure 10. Equivalent circuit diagram of electrode reaction under a fixed cathodic polarization potential

It can be concluded from Figure 8(a) that charge transfer resistance (R_t) increases rapidly at first and then decreases with the negative shift of the cathodic polarization potential in Korla simulated soil solution environment. The relationship between the polarization potential and R_t is expressed by equation (3) when the polarization potential has not reach to the maxima value (greater than -800 mV); The relationship between them is described by equation (4) when polarization potential is smaller than -800 mV. At this juncture the hydrogen evolution reaction is a small part in the total cathode reaction which implies $R_{t,H} \rightarrow \infty$, $R_{t,c}$ is almost the same as $R_{t,o}$ (transfer resistance) and $R_{t,c}$ decreases gradually with the negative shift of cathode potential. However with the increase in the hydrogen evolution during the process, $R_{t,H}$ becomes smaller and it will affect $R_{t,c}$ which would decrease rapidly and lead to an inflection point on the R_t -E curve which is just the point for potential of hydrogen evolution. Therefore the X100 steel’s hydrogen evolution potential under Korla simulated soil solution environment is -925 mV and the optimum cathodic protection potential is -800 mV.

As can be seen from Figure 8(b), the R_t -E curve of X100 steel under Lhasa simulated soil solution environment has similar trends as that under Korla simulated soil solution environment. R_t rapidly increases to a maximum value at first and then it reduces with the negative shift of the cathodic

protection potential. It can be concluded that the relationship between R_i and polarization potential can be expressed by equation (3) before the potential reaching a maximum value of -850mV and the remaining process can be expressed by equation (4). Therefore X100 steel's hydrogen evolution potential under Lhasa simulated soil solution environment is -975 mV and the optimum cathodic protection potential is -850 mV .

Similarly, from the R_i - E curve in Yingtan simulation soil solution of Figure 8(c), it can be seen that the relationship between R_i and polarization potential can be explained by equation (3) before the potential value is greater than -875mV before the extreme point appears. Within the range of less than -875 mV the equation (4) is used for analysis. It can be seen that the X100 steel's optimum cathodic protection potential is -875 mV and the hydrogen evolution potential is -1000 mV in Yingtan simulated soil solution environment. Therefore, the optimum protection potential and hydrogen evolution potential of X100 steel in Korla, Lhasa, and Yingtan simulated soil solutions are shown in Figure 11.

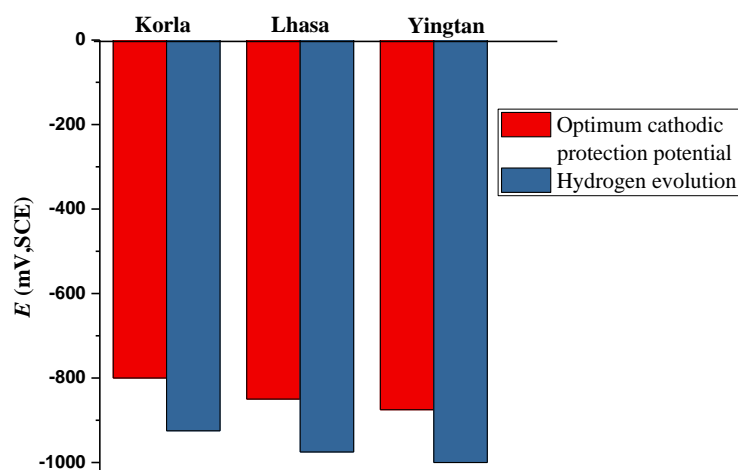


Figure 11. Optimum cathodic protection potential and hydrogen evolution potential of X100 steel in three simulated soil solutions

Li [27] studied the electrochemical impedance spectrum characteristics of carbon steel in soils with different levels of humidity. The equivalent circuit model of carbon steel corrosion in soil was put forward and the influence of soil moisture on corrosion electrochemistry of carbon steel was also discussed. Despite these studies, the existing research on the cathodic protection of buried pipeline is mainly aimed at low strength pipeline steel and the cathodic protection potential generally has the experience value of -850mV [16] which is not effective for the best cathodic protection potential of X100 high strength pipeline steel. If only relying on the traditional (-850mV) cathodic protection potential in different soil environments, the X100 pipe steel will be under-protected or over-protected, and the ideal cathodic protection effect will not be achieved.

In this experiment, the optimal cathodic protection potential and hydrogen evolution potential of X100 steel in different soil simulation solutions were quickly and accurately determined by planning curve and electrochemical impedance spectroscopy. By combining the experimental phenomena and the hydrogen evolution potential shown in Figure 11, it can be concluded that when $R_t < 1000 \Omega \cdot \text{cm}^2$ the hydrogen evolution starts to generate few bubbles; when $R_t < 600 \Omega \cdot \text{cm}^2$ the hydrogen evolution becomes very notable and generates more bubbles; when $R_t < 150 \Omega \cdot \text{cm}^2$ the hydrogen evolution is violent. This observation confirms that at $R_t < 1000 \Omega \cdot \text{cm}^2$, the cathode potential is just the hydrogen evolution potential.

The R_t -E curve has four parts: the first has the largest slope which is from the self-corrosion potential to the optimum cathodic protection potential, the second has a larger slope which is from the optimum cathodic protection potential to the hydrogen evolution's potential, the third has the smaller slope which is from the hydrogen's origin potential to the obvious hydrogen's potential, and the last is almost one line with a slope almost to zero, which representing an obvious hydrogen evolution reaction.

4. CONCLUSIONS

(1) The polarization curves of X100 steel in Korla, Lhasa, and Yingtian stations have similar trends. There are two inflection points. The cathode response before the first inflection point is mainly the reduction reaction of oxygen, and the second inflection point is the evolution of hydrogen starting potential.

(2) When $R_t < 1000 \Omega \cdot \text{cm}^2$, hydrogen evolution starts to emerge. When $R_t < 600 \Omega \cdot \text{cm}^2$, the hydrogen evolution would become obvious. When $R_t < 150 \Omega \cdot \text{cm}^2$, the hydrogen evolution would clearly occur.

(3) According to the experimental results, there are four parts in the curves: the first has the largest slope which is from the self-corrosion potential to the optimum cathodic protection potential, the second has a larger slope which is from the optimum cathodic protection potential to the hydrogen evolution's potential, the third has a smaller slope which is from the hydrogen's origin potential to the obvious hydrogen's potential, and the last is almost one line with a slope almost to zero, which representing an obvious hydrogen evolution reaction.

(4) Combining the R_t -E and polarization curves can assist in making sure that the potential of hydrogen reaction and the optimum cathodic protection potential under three kinds of soil solution environments are simulated correctly. The cathodic protection potential and the hydrogen evolution potential are found to be in the order: Korla Station > Lhasa Station > Yingtian Station.

ACKNOWLEDGEMENTS

This study is supported by National Natural Science Foundation of China (No. 51471011) and "Rixin Scientist" of Beijing University of Technology.

References

1. X. Li, Q. J. Zhu and N. Zhou, *Surf. Tech.*, 12 (2017) 206.
2. C. M. Xu, *J. Iron & Steel Research.*, 23 (2011) 25.
3. X. Wang, X. Tang and L. Wang, *Int. J. Electrochem. Sci.*, 9 (2014) 4574.
4. L. Y. Xu and Y. F. Cheng, *Corros. Sci.*, 64 (2012) 145.
5. X. Wang, C. Wang and D. Wang, *J. Chin. Uni. Petrol.*, 39 (2015) 142.
6. X. T. Zha, Zhang. J. W and S. L. Chen, *Surf. Tech.*, 44 (2015) 12.
7. L. Zhou, W. L. Tao and L. J. Li, *Surf. Tech.*, 44 (2015) 118.
8. I. M. Gadala, M. A. Wahab and A. Alfantazi, *Mater. Design.*, 97 (2016) 287.
9. P. V. Sklyuev, *Met. Sci. Heat. Treat.*, 10 (1968) 492.
10. F. Mahdavi, M. Forsyth and M. Y. J. Tan, *Prog. Org. Coat.*, 103 (2017) 83.
11. M. Mahdavian, R. Naderi and M. Peighambari, *J. Ind. Eng. Chem.*, 21 (2014) 1167.
12. P. Pedefferri, *Constr. Build. Mater.*, 10 (1996) 391.
13. T. Kamimura and H. Kishikawa, *Corros.*, 54 (1998) 979.
14. L. Nielsen, and F. Galsgaard, Sensor Technology for On-Line Monitoring of AC Induced Corrosion Along Pipelines, NACE Corrosion/2005, Houston TX, USA, 2005, Paper No. 05375.
15. X. Chen and X. G. Li, *Corro. Sci.*, 51 (2009) 2242.
16. M. Oonishi, *Boosei Kanri.*, 20 (1976) 24.
17. G. H. Zhang, M. Gong and Q. Tang, *Corros. Prot.*, 32 (2011) 868.
18. L. Zhang, H. J. Shen and J. Y. Sun, *Mater. Chem. Phys.*, 207 (2018) 123.
19. G. A. El-Mahdy, A. Nishikata and T. Tsuru, *Corros. Sci.*, 42 (2000) 183.
20. C. N. Cao and J. Q. Zhang, An Introduction to Electrochemical Impedance Spectroscopy, Science Press, (2002) Beijing, China.
21. C. F. Dong, A. Q. Fu and X. G. Li, *Electrochim. Acta.*, 54 (2009) 628.
22. N. X. Xu and C. D. Zhang, *Corros Prot.*, 2 (1997) 55.
23. D. A. Aikens, *J. Chem. Educ.*, 60 (2004) 669.
24. Z. L. Li, Q. M. Ding and Y. F. Zhang, *Corros. Prot.*, (2010).
25. J. F. Mansfeld, *Russ. J. Electrochem.*, 36 (2000) 1063.
26. J. U. Rammelt and G. Reinhard, *Prog. Org. Coat.*, 21 (1992) 205.
27. M. C. Li, H. C. Lin and C. N. Cao, *J. Chin. Soc. Corros. Prot.*, 20 (2000) 111.

© 2018 The Authors. Published by ESG (www.electrochemsci.org). This article is an open access article distributed under the terms and conditions of the Creative Commons Attribution license (<http://creativecommons.org/licenses/by/4.0/>).